

Wave fields in the stratified fluid-saturated porous half-space induced by dislocation sources

YOUSHUO SONG, JIANCHENG SHI

*Department of Mechanical Engineering
University of Shanghai for Science and Technology
Shanghai 200093, China
e-mail: wssys2006@163.com*

IN THIS STUDY, THE WAVE FIELDS induced by both tensile and shear displacement dislocations in stratified fluid-saturated porous media are computed by using the reflection and transmission matrix method. The components of the source discontinuity vector across the source plane to describe those tensile and shear faults are explicitly displayed by using the surface vector harmonics. Numerical examples for a two layer model subjected to tensile and shear dislocations are provided. From the waveforms of surface displacements, the arrivals of transmitted and converted *PS* and *SP* waves at the interface of the two layer model can be clearly observed.

Key words: tensile dislocation, shear dislocation, stratified media, wave propagation.

Copyright © 2017 by IPPT PAN

1. Introduction

MANY GEOMATERIALS SUCH AS SOIL AND ROCKS usually contain pore fluids, and therefore can be approximately considered as fluid-saturated porous media. Frenkel may be the first who investigated the wave phenomena in saturated porous media. Afterwards, BIOT [1–4] established the general theory for modelling wave propagation in the saturated media. Based on Biot's theory, several papers have appeared on the wave propagation in a stratified isotropic homogeneous poroelastic medium, see, for example, RAJAPAKSE and SENJUNTICHAI [5], LU and HANYGA [6], MESGOUEZ *et al.* [7], ZHENG *et al.* [8], and ZHENG and DING [9]. Today, however, most of previously published works concerned the displacement fields produced by point forces in the layered media, and wave fields induced by dislocation sources in stratified poroelastic media have not been studied before.

The determination of static and dynamic displacement fields induced by dislocation sources in stratified media has long been a subject of interest in geophysics and seismology [10]. Based on quasi-static Biot's theory [11], PAN [12] first investigated static point dislocations in the stratified proelastic half-space using surface vector harmonics [13]. Recently, ZHENG and DING [14] have extended the Pan's study of static dislocations in fluid-saturated solids to the case

of dynamic dislocations based on Biot's dynamic theory [3–4]. In their work, the general point dislocation source in saturated media is described by discontinuities in related physical quantities, such as displacement, stress, etc., across a horizontal plane.

The aim of the present study is to study the wave fields induced by tensile and shear displacement point dislocations in the stratified saturated media by using the reflection and transmission matrix method [15]. The components of the source discontinuity vector across the source plane to represent those point displacement dislocations will be explicitly displayed by using the surface vector harmonics. The derived surface displacement fields expressed in terms of Hankel-type integrals will be evaluated using the discrete wave number integration method of BOUCHON [16].

2. Surface vector harmonics and first-order ordinary differential equations

Based on Biot's dynamic poroelasticity [3–4], the equations of motions for an isotropic fluid-saturated porous solid can be written in the frequency domain as [9]

$$(2.1) \quad (\lambda + 2\mu)\nabla\nabla \cdot \mathbf{u} - \mu\nabla \times \nabla \times \mathbf{u} + \omega^2 \left(\rho - \frac{\rho_f^2}{\rho_m} \right) \mathbf{u} - \left(\alpha - \frac{\rho_f}{\rho_m} \right) \nabla p = \mathbf{0},$$

$$(2.2) \quad \nabla^2 p + \frac{\omega^2 \rho_m}{M} p - \omega^2 (\rho_f - \alpha \rho_m) \nabla \cdot \mathbf{u} = 0,$$

where \mathbf{u} is the solid displacement vector, p denotes the pore pressure, μ is the shear modulus of the solid frame, the drained Lamé constant λ is given by $\lambda = K - 2/3\mu$, where K is the drained bulk modulus of the solid frame, and the Biot–Willis coefficient [17] α , the coupling modulus M are given by

$$(2.3) \quad \alpha = 1 - \frac{K}{K_s},$$

$$(2.4) \quad M = \left[\frac{\alpha - \phi}{K_s} + \frac{\phi}{K_f} \right]^{-1},$$

where ϕ is the porosity, K_f and K_s are the bulk moduli of the fluid and the solid phases, respectively. ρ_f and ρ are the densities of the pore fluid and the bulk materials, where $\rho = \phi\rho_f + (1 - \phi)\rho_s$ with ρ_s being the density of the grain material, and ρ_m is defined as

$$(2.5) \quad \rho_m = m - \frac{i}{\omega} \frac{\eta}{\kappa},$$

where $m = \rho_f a_\infty / \phi$ with a_∞ being tortuosity. The viscosity is denoted as η , and the permeability is κ . The permeability is generally frequency dependent, but here a frequency independent value is taken which is valid at the low-frequency range, i.e.,

$$(2.6) \quad \omega \ll \omega_c,$$

where ω_c is the so-called Biot critical frequency [4]

$$(2.7) \quad \omega_c = \frac{\eta\phi}{a_\infty\kappa\rho_f}.$$

Typically, ω_c is on the order of megahertz (MHz) in rocks and sand [18].

It should be remarked that alternatively the governing equations for Biot's equations can be formulated in terms of the solid displacement \mathbf{u} and the relative fluid-solid displacement \mathbf{w} (see, e.g., ZHENG and DING [19]).

In a cylindrical coordinate system ($\mathbf{e}_r, \mathbf{e}_\theta, \mathbf{e}_z$), we introduce three orthogonal vectors [9, 12, 13]:

$$(2.8) \quad \begin{aligned} \mathbf{R}_k^m &= Y_k^m \mathbf{e}_z, \\ \mathbf{S}_k^m &= \frac{1}{k} \frac{\partial Y_k^m}{\partial r} \mathbf{e}_r + \frac{1}{kr} \frac{\partial Y_k^m}{\partial \theta} \mathbf{e}_\theta, \\ \mathbf{T}_k^m &= \frac{1}{kr} \frac{\partial Y_k^m}{\partial \theta} \mathbf{e}_r - \frac{1}{k} \frac{\partial Y_k^m}{\partial r} \mathbf{e}_\theta, \end{aligned}$$

where

$$(2.9) \quad Y_k^m(r, \theta) = J_m(kr) e^{im\theta}, \quad m = 0, \pm 1, \pm 2, \dots,$$

and $J_n(\xi)$ denotes the Bessel function of the first kind of order n .

Then, the solid displacement \mathbf{u} , the traction on the horizontal plane \mathbf{T} , the pore pressure p , and the fluid discharge in the z -direction q_z can be expanded in terms of [9, 12]

$$(2.10) \quad \mathbf{u}(r, \theta, z, \omega) = \frac{1}{2\pi} \sum_{m=-\infty}^{\infty} \int_0^{\infty} (U_R \mathbf{R}_k^m + U_S \mathbf{S}_k^m + U_T \mathbf{T}_k^m) k dk,$$

$$(2.11) \quad \mathbf{T}(r, \theta, z, \omega) = \sigma \cdot \mathbf{e}_z = \frac{1}{2\pi} \sum_{m=-\infty}^{\infty} \int_0^{\infty} (T_R \mathbf{R}_k^m + T_S \mathbf{S}_k^m + T_T \mathbf{T}_k^m) k dk,$$

$$(2.12) \quad p(r, \theta, z, \omega) = \frac{1}{2\pi} \sum_{m=-\infty}^{\infty} \int_0^{\infty} P Y_k^m k dk,$$

$$(2.13) \quad q_z(r, \theta, z, \omega) = \frac{1}{2\pi} \sum_{m=-\infty}^{\infty} \int_0^{\infty} Q_z Y_k^m k dk.$$

Under these expansions, the second-order differential equations of motion (2.1) and (2.2) are reduced to two independent sets of first-order ordinary differential equations. Both of the two sets of equations can be written in the form [13, 15]

$$(2.14) \quad \frac{d}{dz} \mathbf{B}(z) = \omega \mathbf{A} \mathbf{B}(z),$$

where \mathbf{B} is the generalized stress-displacement vector which takes the form: for P - SV waves

$$(2.15) \quad \mathbf{B}_P = [U_R, U_S, -i\omega^{-1}Q_z, \omega^{-1}T_R, \omega^{-1}T_S, \omega^{-1}P]^T,$$

and for SH waves

$$(2.16) \quad \mathbf{B}_H = [U_T, \omega^{-1}T_T]^T.$$

For P - SV waves, the coefficient matrix \mathbf{A} has the form [9]

$$(2.17) \quad \mathbf{A}_P = \begin{bmatrix} 0 & \frac{\lambda}{\lambda + 2\mu} p & 0 & \frac{1}{\lambda + 2\mu} & 0 & \frac{\alpha}{\lambda + 2\mu} \\ -p & 0 & 0 & 0 & \frac{1}{\mu} & 0 \\ 0 & \left(\frac{2\alpha\mu}{\lambda + 2\mu} + \Lambda_3 \right) p & 0 & -\frac{\alpha}{\lambda + 2\mu} & 0 & \frac{p^2}{\rho_m} - \frac{\lambda_c + 2\mu}{M(\lambda + 2\mu)} \\ -\rho & 0 & -\rho_f & 0 & p & 0 \\ 0 & \frac{4\mu(\lambda + \mu)}{\lambda + 2\mu} p^2 - \rho_3 & 0 & -\frac{\lambda}{\lambda + 2\mu} p & 0 & \left(\frac{2\alpha\mu}{\lambda + 2\mu} + \Lambda_3 \right) p \\ \rho_f & 0 & \rho_m & 0 & 0 & 0 \end{bmatrix},$$

where p is the slowness ($\omega p = k$), and

$$(2.18) \quad \lambda_c = \lambda + \alpha^2 M,$$

$$(2.19) \quad \rho_3 = \rho \left(1 - \frac{\rho_f^2}{\rho \rho_m} \right),$$

$$(2.20) \quad \Lambda_3 = -\frac{\rho_f}{\rho_m}.$$

For SH waves, \mathbf{A} is given by

$$(2.21) \quad \mathbf{A}_H = \begin{bmatrix} 0 & \frac{1}{\mu} \\ \mu p^2 - \rho_3 & 0 \end{bmatrix}.$$

3. Representation of general point dislocations

The plane Σ through the point dislocations with normal \mathbf{v} is called the fault plane or dislocation plane, and it has two adjacent surfaces labelled as Σ^+ and Σ^- . The normal to Σ is \mathbf{v} , pointing from Σ^- to Σ^+ (see Fig. 1 [14]). The most general point dislocations, across an element of arbitrary surface Σ at $x_3 = z_s$ with the normal \mathbf{v} , in fluid-saturated porous solids can be represented by

$$(3.1) \quad \begin{aligned} [u_i](\mathbf{x}, \omega) &= a_i \delta(x_1) \delta(x_2), \\ [\sigma_{ik}](\mathbf{x}, \omega) v_k &= b_i \delta(x_1) \delta(x_2), \\ [q_k](\mathbf{x}, \omega) v_k &= c \delta(x_1) \delta(x_2), \\ [p](\xi, \omega) &= d \delta(x_1) \delta(x_2), \end{aligned}$$

where $[u_i](\mathbf{x}, \omega)$, $[\sigma_{ik}](\mathbf{x}, \omega)$, $[q_k](\mathbf{x}, \omega)$ and $[p](\mathbf{x}, \omega)$ are the discontinuities in displacement, stress, fluid discharge, and pore pressure across Σ and defined by $[u_i](\mathbf{x}, \omega) = u_i(\mathbf{x}, \omega)|_{\Sigma^+} - u_i(\mathbf{x}, \omega)|_{\Sigma^-}$, etc. In addition, a_i , b_i , c , d are functions of ω .

In order to use the matrix theory to calculate the wave fields induced by dislocation sources (3.1) in a stratified medium, it is necessary to represent the sources in terms of discontinuities in components of the generalized stress-displacements vector across the horizontal plane. Using the body-force and fluid-source equivalents for dynamic dislocations, we can find the components of the source discontinuity vector, that is

$$(3.2) \quad \mathbf{S}(z_s) = \mathbf{B}(z_{s+}) - \mathbf{B}(z_{s-}),$$

to represent the general point dislocations (3.1), and they are [14]

$$\begin{aligned} [U_R]_{-}^{+} &= \frac{1}{\lambda + 2\mu} (2\mu a_3 v_3 + \lambda a_k v_k), & m = 0, \\ [U_S]_{-}^{+} &= \frac{1}{2} (\pm (a_1 v_3 + a_3 v_1) - i (a_2 v_3 + a_3 v_2)), & m = \pm 1, \\ [U_T]_{-}^{+} &= \frac{1}{2} (\mp (a_2 v_3 + a_3 v_2) - i (a_1 v_3 + a_3 v_1)), & m = \pm 1, \\ [\omega^{-1} T_R]_{-}^{+} &= \omega^{-1} b_3, & m = 0, \\ [\omega^{-1} T_S]_{-}^{+} &= \frac{\mu(3\lambda + 2\mu)}{\lambda + 2\mu} p (a_1 v_1 + a_2 v_2), & m = 0, \\ &= \frac{1}{2} \omega^{-1} (\pm (b_1 - \Lambda_3 d v_1) - i (b_2 - \Lambda_3 d v_2)), & m = \pm 1, \\ &= \frac{\mu}{2} p ((a_2 v_2 - a_1 v_1) \pm i (a_1 v_2 + a_2 v_1)) & m = \pm 2, \end{aligned}$$

$$\begin{aligned}
[\omega^{-1}T_T]_{-}^{+} &= \frac{1}{2}\omega^{-1}(-i(b_1 - A_3dv_1)b_1 \mp (b_2 - A_3dv_2)), & m = \pm 1, \\
&= \frac{\mu}{2}p(\pm i(a_1v_1 - a_2v_2) + (a_1v_2 + a_2v_1)) & m = \pm 2, \\
[\omega^{-1}P]_{-}^{+} &= \omega^{-1}dv_3, & m = 0, \\
[-i\omega^{-1}Q]_{-}^{+} &= -i\omega^{-1}c + \alpha a_k v_k, & m = 0, \\
(3.3) \qquad &= \frac{p}{2} \frac{d}{\omega \rho_m} (\mp v_1 + iv_2), & m = \pm 1.
\end{aligned}$$

4. Point displacement dislocations

Since the determination of displacement fields produced by displacement discontinuities is of fundamental interest in geophysics and seismology, we focus our discussion on point displacement dislocations, particularly those of shear dislocations. An arbitrary displacement dislocation across an element of surface Σ with the normal \mathbf{v} can be split into two parts, that is

$$(4.1) \qquad [\mathbf{u}] = [u_1]\mathbf{v} + [u_2]\mathbf{e}, \qquad (\mathbf{v} \cdot \mathbf{e} = \mathbf{0}).$$

As it is shown in (4.1), the displacement component $[u_1]$ is perpendicular to the dislocation surface (that is, along the direction of the normal \mathbf{v}), and the other component $[u_2]$ is parallel to the dislocation surface. If displacement discontinuity occurs along the direction of the normal \mathbf{v} , such discontinuity is termed tensile dislocation. On the other hand, displacement discontinuity occurred parallel to the dislocation surface is termed shear dislocation.

4.1. Tensile dislocation

We begin by considering a tensile fault embedded in a poroelastic medium. In Cartesian coordinates (x, y, z) , related to cylindrical coordinates (r, θ, z) via $x = r \cos \theta$, $y = r \sin \theta$, we define a tensile dislocation located at $(x = 0, y = 0, z = h)$ with a dip angle δ and magnitude U_0 , as shown in Fig. 1. The dip angle δ ($0 \leq \delta \leq \pi/2$) is defined as the angle that the dislocation plane makes with the horizontal plane through the dislocation source. A fault has two surfaces, and the one illustrated in Fig. 1 is the surface Σ^+ . From Fig. 1, the unit normal \mathbf{v} of dislocation plane Σ is

$$(4.2) \qquad \mathbf{v} = (0, -\sin \delta, \cos \delta)^T.$$

Therefore, by using (3.3) it can be found that the nonzero components of the source discontinuity vector \mathbf{S} corresponding to the tensile dislocation with unit magnitude are

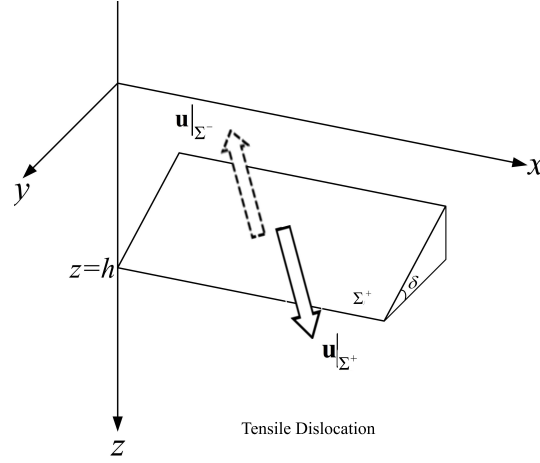


FIG. 1. Geometry of an arbitrary tensile dislocation $[\mathbf{u}] = U_0 \mathbf{v}$ in Cartesian coordinates (x, y, z) . The heavy arrow shows the motion on the side Σ^+ , and the broken arrow shows the motion on the side Σ^- .

$$\begin{aligned}
 [U_R]_{\pm}^{\pm} &= \frac{1}{\lambda + 2\mu} (\lambda + 2\mu \cos^2 \delta), & m = 0, \\
 [U_S]_{\pm}^{\pm} &= \frac{i}{2} \sin 2\delta, & m = \pm 1, \\
 [U_T]_{\pm}^{\pm} &= \pm \frac{1}{2} \sin 2\delta, & m = \pm 1, \\
 [\omega^{-1} T_S]_{\pm}^{\pm} &= \frac{\mu(3\lambda + 2\mu)}{\lambda + 2\mu} p \sin^2 \delta, & m = 0, \\
 &= \frac{\mu}{2} p \sin^2 \delta, & m = \pm 2, \\
 [\omega^{-1} T_T]_{\pm}^{\pm} &= \mp i \frac{\mu}{2} p \sin^2 \delta, & m = \pm 2, \\
 [-i\omega^{-1} Q]_{\pm}^{\pm} &= \alpha, & m = 0.
 \end{aligned}
 \tag{4.3}$$

4.2. Shear dislocation

Next we consider a shear fault embedded in a poroelastic medium. In the case of a shear dislocation, besides the dip angle δ , another fault parameter φ is introduced to describe the fault, as shown in Fig. 2. The slip angle φ ($0 \leq \varphi \leq 2\pi$) used to specify the direction of slip and defined as the angle that the slip vector \mathbf{e} makes with the strike direction which is taken as the x direction in Fig. 2. From Fig. 2, the unit slip vector \mathbf{e} parallel to the dislocation surface Σ is

$$\mathbf{e} = (\cos \varphi, -\sin \varphi \cos \delta, -\sin \varphi \sin \delta)^T.
 \tag{4.4}$$

Substituting (4.2) and (4.4) into (3.3), one can find the nonzero components of the source discontinuity vector \mathbf{S} corresponding to the arbitrarily oriented shear dislocation with unit magnitude. They are

$$\begin{aligned}
 [U_R]_{-}^{+} &= -\frac{\mu}{\lambda + 2\mu} \sin \varphi \sin 2\delta, & m = 0, \\
 [U_S]_{-}^{+} &= \frac{1}{2}(\pm \cos \varphi \cos \delta + i \sin \varphi \cos 2\delta), & m = \pm 1, \\
 [U_T]_{-}^{+} &= \frac{1}{2}(\pm \sin \varphi \cos 2\delta - i \cos \varphi \cos \delta), & m = \pm 1, \\
 [\omega^{-1}T_S]_{-}^{+} &= \frac{\mu(3\lambda + 2\mu)}{2(\lambda + 2\mu)} p \sin \varphi \sin 2\delta, & m = 0, \\
 &= \frac{\mu}{4} p (\sin \varphi \sin 2\delta \mp 2i \cos \varphi \sin \delta), & m = \pm 2, \\
 (4.5) \quad [\omega^{-1}T_T]_{-}^{+} &= \frac{\mu}{4} p (\mp i \sin \varphi \sin 2\delta - 2 \cos \varphi \sin \delta), & m = \pm 2.
 \end{aligned}$$

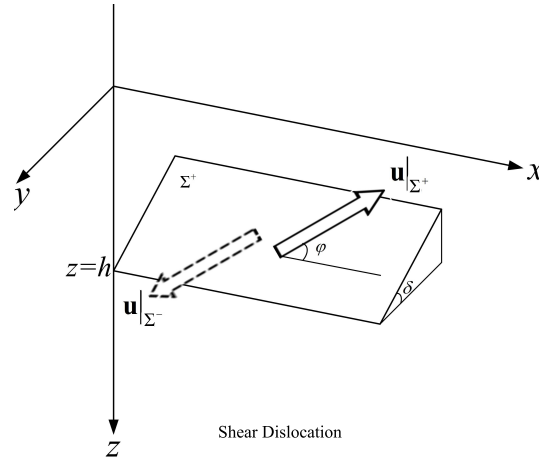


FIG. 2. Geometry of an arbitrary tensile dislocation $[\mathbf{u}] = U_0 \mathbf{e}$ in Cartesian coordinates (x, y, z) , where \mathbf{e} is the slip vector parallel to the dislocation surface. The angle φ is known as the slip angle.

It should be mentioned that the so-called three fundamental shear dislocations are the vertical strike-slip fault ($\delta = \pi/2, \varphi = 0$), the vertical dip-slip fault ($\delta = \pi/2, \varphi = \pi/2$), and the 45° dip-slip fault ($\delta = \pi/4, \varphi = \pi/2$).

5. Surface displacement of the stratified fluid-saturated half-space

Consider a semi-infinite poroelastic medium consisting of $n - 1$ parallel, homogeneous layers laying over a homogeneous half-space. The layers are numbered

serially, the topmost layer being layer 1 and the half-space layer n . The origin of the cylindrical coordinate system (r, θ, z) is placed at the surface with the z -axis drawn downwards into the medium. The k -th layer is of thickness d_k and is bounded by the interface z_k, z_{k+1} . The source (e.g., a shear dislocation) is presumed to be located in the k -th layer and is at a depth z_s from the top interface (Fig. 3).

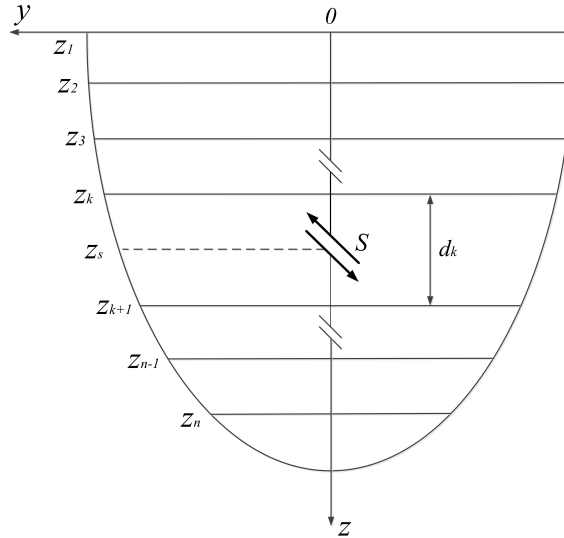


FIG. 3. Configuration of a multilayered poroelastic half-space.

Using the generalized reflection and transmission matrix method, we can obtain the displacement fields in the stratified medium, particularly the surface displacement [9, 15]:

$$(5.1) \quad \mathbf{W}_0 = (\mathbf{m}_U^0 + \mathbf{m}_D^0 \tilde{\mathbf{R}})[\mathbf{I} - \mathbf{R}_D^{0L} \tilde{\mathbf{R}}]^{-1} \boldsymbol{\sigma}(z_s),$$

where $\mathbf{m}_U^0, \mathbf{m}_D^0, \tilde{\mathbf{R}}, \mathbf{R}_D^{0L}, \tilde{\mathbf{R}}$ are matrixes, \mathbf{I} is a unit matrix, and $\boldsymbol{\sigma}(z_s)$ is a vector. Detailed definitions and explicit expressions of these matrixes and the vector have been given in KENNETT [15]. In the subsequent numerical examples, the approximate formula

$$(5.2) \quad \mathbf{W}_0^{(0)} = (\mathbf{m}_U^0 + \mathbf{m}_D^0 \tilde{\mathbf{R}}) \mathbf{T}_U^{0S} (\mathbf{R}_D^{SL} \Sigma_D - \Sigma_U),$$

which corresponds to the direct propagation from a buried source to the surface without any multiples being included, is also used for computing the surface displacement.

In addition, the expression for the displacement fields in the stratified medium can be found in ZHENG and DING [9].

6. Numerical examples

Once solutions for the generalized stress-displacement vectors are known, the displacements are recovered using

$$(6.1) \quad u_r(r, \theta, z, \omega) = \frac{1}{2\pi} \int_0^\infty dk k \sum_{m=-2}^2 \left[U_S(k, m, z, \omega) \frac{\partial J_m(kr)}{\partial(kr)} + U_T(k, m, z, \omega) \frac{im}{kr} J_m(kr) \right] e^{im\theta},$$

$$(6.2) \quad u_\theta(r, \theta, z, \omega) = \frac{1}{2\pi} \int_0^\infty dk k \sum_{m=-2}^2 \left[U_S(k, m, z, \omega) \frac{im}{kr} J_m(kr) - U_T(k, m, z, \omega) \frac{\partial J_m(kr)}{\partial(kr)} \right] e^{im\theta},$$

$$(6.3) \quad u_z(r, \theta, z, \omega) = \frac{1}{2\pi} \int_0^\infty dk k \sum_{m=-2}^2 U_R(k, m, z, \omega) J_m(kr) e^{im\theta}.$$

Such Hankel-type integrals are evaluated by using the discrete wave number method [16]. The time domain solutions for a time-dependent dislocation source can be built from the frequency domain solutions (6.1), (6.2) and (6.3) using the discrete Fourier transform.

As an example, a two layer model with a 0.5-km-thick sand layer overlying a sandstone half-space is chosen. The medium properties are listed in Table 1. The material parameters in Table 1 are taken from the reference by ZHENG and DING [9]. The point dislocations are all located on the coordinate axis $r = 0$ at the depth $z_S = 1$ km. The source time function used in all subsequent examples is a 20 Hz Ricker wavelet.

Table 1. Properties of the homogeneous porous layers used in the numerical calculations.

Properties	Sand	Sandstone
Porosity ϕ	0.3	0.065
Permeability κ_0 , m ²	10 ⁻¹¹	10 ⁻¹³
Solid bulk modulus K_s , GPa	35	36
Fluid bulk modulus K_f , GPa	2.2	2.2
Frame bulk modulus K , GPa	5.0	25.0
Frame shear modulus μ , GPa	3.0	18.0
Fluid viscosity η , Pas	10 ⁻³	10 ⁻³
Solid grain density ρ_s , kg/m ³	2300	2600
Fluid density ρ_f , kg/m ³	10 ³	10 ³
Tortuosity α_∞	3	3

Firstly, we consider tensile dislocations embedded in the two-layer poroelastic half-space. Figures 4 and 5 show the comparison of synthetic seismograms calculated at receiver on the free surface using equation (5.2) (solid line) and equation (5.1) (dash line) due to a horizontal ($\delta = 0$) and 45° ($\delta = \pi/4$) tensile dislocation, respectively. In the first case, the displacement fields are axisymmetric with

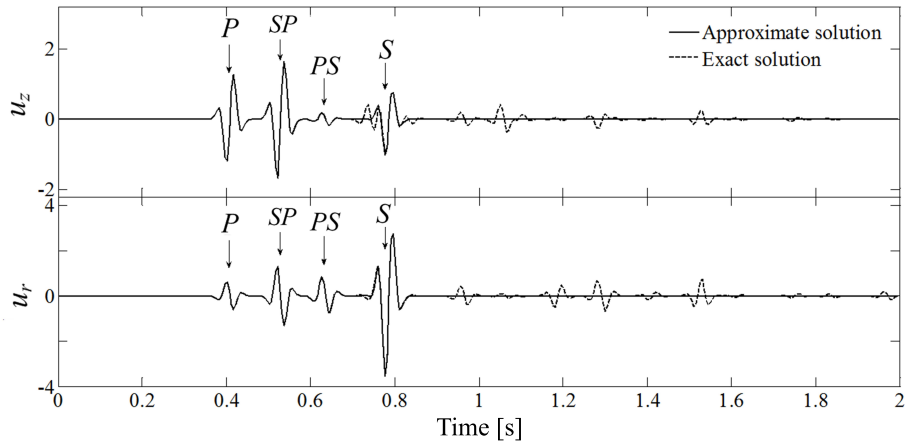


FIG. 4. Waveforms of surface displacements radiated by a tensile fault ($\delta = 0$) buried at depth $z_S = 1$ km. The receiver is located at $\mathbf{x}_R = (1 \text{ km}, 0)$.

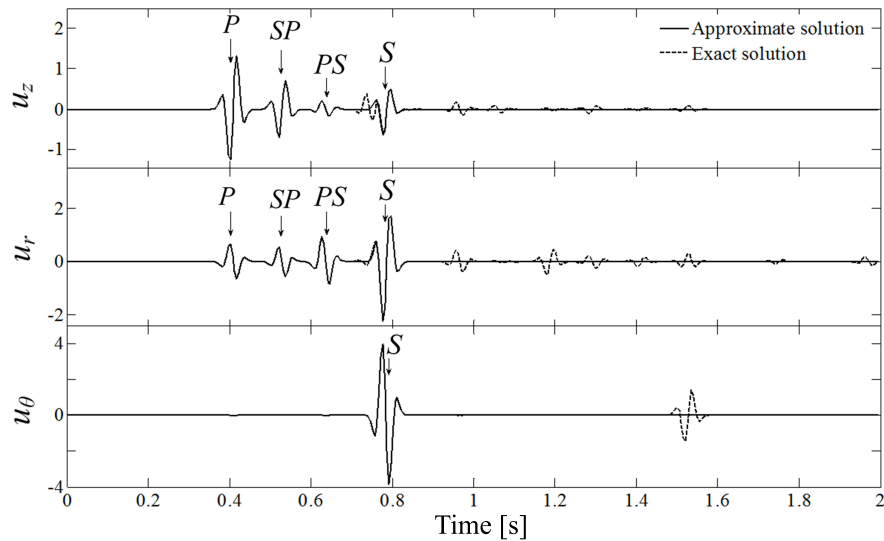


FIG. 5. Waveforms of surface displacements radiated by a tensile fault ($\delta = \pi/4$) buried at depth $z_S = 1$ km. The receiver is located at $\mathbf{x}_R = (1 \text{ km}, 22.5^\circ, 0)$.

respect to the z -axis, and thus, u_θ vanish and $u_r(r, z)$, $u_z(r, z)$ are independent of θ . As expected, only four arrivals corresponding to transmitted P , S waves,

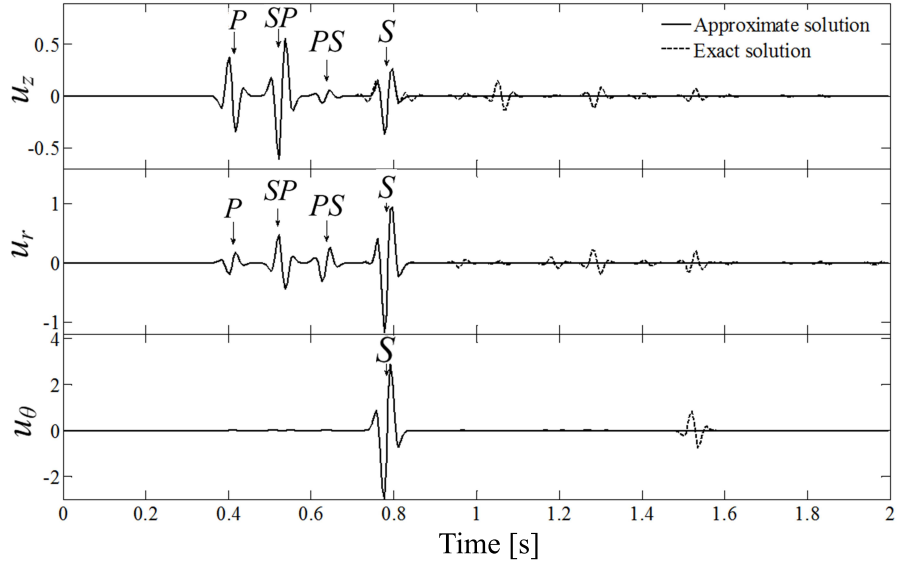


FIG. 6. Waveforms of surface displacements radiated by the vertical strike-slip fault buried at depth $z_S = 1$ km. The receiver is located at $\mathbf{x}_R = (1 \text{ km}, 22.5^\circ, 0)$.

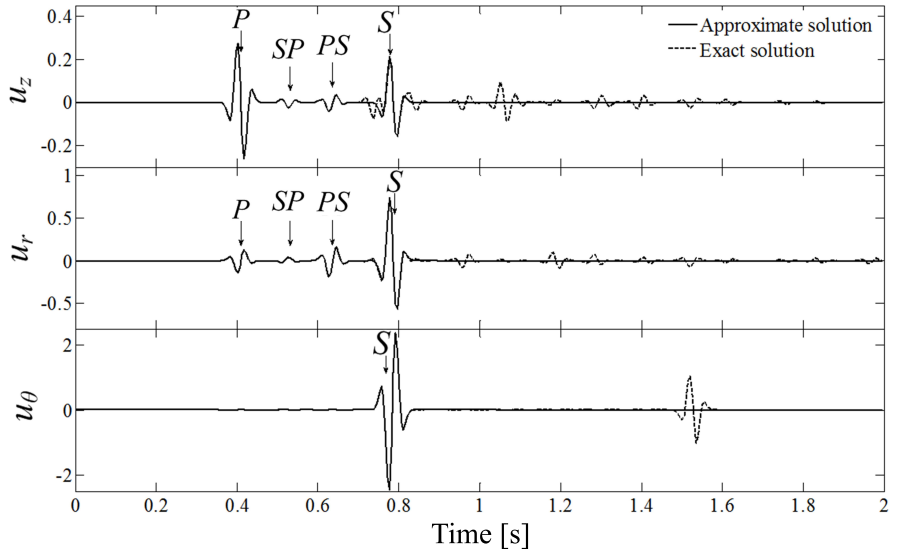


FIG. 7. Waveforms of surface displacements radiated by the vertical dip-slip fault buried at depth $z_S = 1$ km. The receiver is located at $\mathbf{x}_R = (1 \text{ km}, 22.5^\circ, 0)$.

and transmitted and converted PS , SP waves at the interface $z_1 = 0.5$ km are clearly observable from Figs. 4 and 5 by using the approximate formula (5.2). The effects of free surface, giving rise to additional arrivals, can also be clearly observable from Figs. 4 and 5 by using the exact solution (5.1). It can also be noted in these figures that the dominant contributions to azimuthal displacements come from transmitted S waves, and hence, the arrivals of transmitted P , transmitted and converted PS and SP waves can hardly be observable.

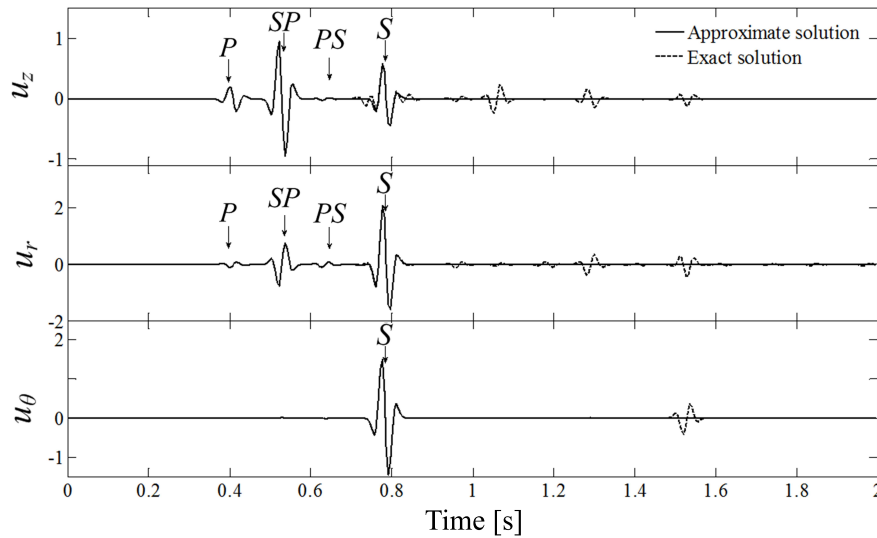


FIG. 8. Waveforms of surface displacements radiated by the 45° dip-slip fault buried at depth $z_S = 1$ km. The receiver is located at $\mathbf{x}_R = (1 \text{ km}, 22.5^\circ, 0)$.

Next, we consider three fundamental shear dislocations buried, respectively, in the stratified media. The resulting surface displacements are shown in Figs. 6–8 for the vertical strike-slip fault, the vertical dip-slip fault and the 45° dip-slip fault, respectively. In these cases, transmitted S waves are the dominant contributions to azimuthal displacements and the contributions from transmitted P , transmitted and converted PS and SP waves are so small that the arrivals of them can hardly be observable from these figures.

7. Conclusions

We have used the reflection and transmission matrix method to compute the surface displacement induced by tensile and shear dislocations in the stratified fluid-saturated poroelastic half-space. We have explicitly displayed the components of the source discontinuity vector across the source plane to describe those

tensile and shear faults by using the surface vector harmonics. We have also provided numerical examples for a two layer model subjected to a horizontal and 45° tensile dislocation, and three fundamental shear dislocations, respectively. Numerical results show that the arrivals of transmitted and converted *PS* and *SP* waves at the interface of the two layer model can be clearly observed from the waveforms of surface displacements.

References

1. M.A. BIOT, *Theory of propagation of elastic waves in a fluid-saturated porous solid. I. Low-frequency range*, The Journal of the Acoustical Society of America, **28**, 168–178, 1956.
2. M.A. BIOT, *Theory of propagation of elastic waves in a fluid-saturated porous solid. II. Higher frequency range*, The Journal of the Acoustical Society of America, **28**, 179–191, 1956.
3. M.A. BIOT, *Mechanics of deformation and acoustic propagation in porous media*, Journal of Applied Physics, **33**, 1482–1498, 1962.
4. M.A. BIOT, *Generalized theory of acoustic propagation in porous dissipative media*, Journal of the Acoustical Society of America, **34**, 1254–1264, 1962.
5. R.K.N. RAJAPAKSE, T.J. SENJUNTICHAI, *Dynamic response of a multi-layered poroelastic medium*, Earthquake Engineering & Structural Dynamics, **24**, 703–722, 1995.
6. J.F. LU, A. HANYGA, *Fundamental solutions for a layered porous half space subject to a vertical point force or a point fluid source*, Computational Mechanics, **35**, 376–391, 2005.
7. G. LEFEUVE-MESGOUEZ, A. MESGOUEZ, G. CHIAVASSA, B. LOMBARD, *Semi-analytical and numerical methods for computing transient waves in 2D acoustic/poroelastic stratified media*, Wave Motion, **49**, 667–680, 2012.
8. P. ZHENG, B. DING, S.X. ZHAO, D. DING, *3D dynamic Green's functions in a multi-layered poroelastic half-space*, Applied Mathematical Modelling, **37**, 10203–10219, 2013.
9. P. ZHENG, B. DING, *The generalized reflection and transmission matrix method for wave propagation in stratified fluid-saturated porous media*, Transport in Porous Media, **102**, 185–206, 2014.
10. K. AKI, P.G. RICHARDS, *Quantitative Seismology*, University Science Books, Sausalito, CA, 2002.
11. M.A. BIOT, *General theory of three-dimensional consolidation*, Journal of Applied Physics, **12**, 155–164, 1941.
12. E. PAN, *Green's functions in layered poroelastic half-spaces*, International Journal for Numerical and Analytical Methods in Geomechanics, **23**, 1631–1653, 1999.
13. H. TAKEUCHI, M. SAITO, *Seismic surface waves*, Methods in Computational Physics, **11**, 217–295, 1971.
14. P. ZHENG, B. DING, *Body force and fluid source equivalents for dynamic dislocations in fluid-saturated porous media*, Transport in Porous Media, **107**, 1–12, 2015.
15. B.L.N. KENNETT, *Elastic wave propagation in stratified media*, Advances in Applied Mechanics, **21**, 79–167, 1981.

-
16. M. BOUCHON, *A simple method to calculate Green's functions for elastic layered media*, Bulletin of the Seismological Society of America, **71**, 959–971, 1981.
 17. M.A. BIOT, D.G. WILLIS, *The elastic coefficients of the theory of consolidation*, Journal of Applied Mechanics, **24**, 594–601, 1957.
 18. F. WENZLAU, T.M. MÜLLER, *Finite-difference modeling of wave propagation and diffusion in poroelastic media*, Geophysics, **74**, T55–T66, 2009.
 19. P. ZHENG, B. DING, *Potential method for 3D wave propagation in a poroelastic medium and its applications to Lamb's problem for a poroelastic half-space*, ASCE International Journal of Geomechanics, **16**, 04015048, 2016.

Received May 13, 2017; revised version August 18, 2017.
